EUROPEAN ORGANIZATION FOR NUCLEAR RESEARCH

CERN/EP 87-59
19 February 1987

INCLUSIVE PION PRODUCTION IN 360 GeV/c pp INTERACTIONS

EHS-RCBC Collaboration

Bombay[1]-Budapest[2]-CERN[3]-Chandigarh[4]-Genova[5]-Innsbruck[6]-Japan UG[7]-Madrid[8]-Mons[9]-Moscow[10]-Rutgers[11]-Serpukhov[12]-Tennessee[13]-Vienna[14] Collaboration

J.L. Bailly[9], W. Bartl[14], B. Buschbeck[14], C. Caso[5], H. Dibon[14], F.J. Diez-Hedo[8], B. Epp[6], A. Ferrando[8], F. Fontanelli[5], S.N. Ganguli[1], I.V. Gorelov[10], A. Gurtu[1], R. Hamatsu[7(a)], Ph. Herquet[9], J. Hrubec[3], Y. Iga[7(a)], V. Khalatyan[12], E. Kistenev[12], S. Kitamura[7(a)], J.M. Kohli[4], D. Kuhn[6], J. MacNaughton[14], P.K. Malhotra[1], S. Matsumoto[7(c)], I.S. Mittra[4], L. Montanet[3], G. Neuhofer[3], N. Oshima[7(a)], P. Porth[14], R. Raghavan[1], T. Rodrigo[8], J.M. Salicio[8], J.B. Singh[3], S. Squarcia[5], V. Stopchenko[12], K. Takahashi[7(b)], U. Trevisan[5], T. Tsurugai[7(a)], T. Yamagata[7(a)], G. Zholobov[12] and S.A. Zotkin[10]

1 Tata Institute of Fundamental Research, Bombay, India
2 Central Research Institute for Physics, Budapest, Hungary
3 CERN, European Organization for Nuclear Research, Geneva, Switzerland
4 Panjab University, Chandigarh, India
5 University of Genova and INFN, Genova, Italy
6 Inst. für Experimentalphysik, Innsbruck, Austria(*)
7(a) Tokyo Metropolitan University, Tokyo, Japan
(b) Tokyo University of Agriculture and Technology, Tokyo, Japan
(c) Chuo University, Tokyo, Japan
(d) Hiroshima University, Hiroshima, Japan
8 Junta de Energia Nuclear, Madrid, Spain
9 Université de l'Etat, Faculté des Sciences, Mons, Belgium
10 Moscow State University, Moscow, USSR
11 Rutgers University, New Brunswick, USA
12 Inst. for High Energy Physics, Serpukhov, USSR
13 University of Tennessee, Knoxville, USA
14 Inst. für Hochenergiephysik, Vienna, Austria(*)

Submitted to Zeitschrift für Physik C

(*) Supported by Fonds zur Förderung der Wissensch. Forschung.

EP/2714P/LM/mk

ABSTRACT

In a study of proton-proton interactions at $\sqrt{s}$ = 26 GeV, inclusive distributions of single pions and systems of pions of various charge combinations are presented, as well as the production ratio obtained in association with various trigger particles. The results are compared to current phenomenological models in an attempt to understand multiparticle production in hadron collisions.

1. INTRODUCTION

Attempts at understanding multiparticle production at low transverse momenta in hadronic collisions have gradually led to a quark-parton picture of soft processes which is exploited in various ways by several models. Among the most recent ones, one may mention the Dual Topological Unitarization (DTU) of Capella [1], the Lund string model of Andersson [2], the QCD approach of Gunion [3], the valon model of Hwa [4], and the additive quark model using quark statistics of Anisovich [5]. For a recent review, see [6]. In general single particle distributions are described fairly well by all these models. It has been suggested [7] that the study of pion systems of different charge combinations may provide additional and more stringent tests of specific models. We therefore present in this paper new data obtained with proton-proton interactions at $\sqrt{s}$ = 26 GeV for inclusive particle ratios of pions and systems of pions with various charges using various trigger particles, i.e. particles of well defined nature restricted to particular Feynman x-intervals. The analysis is mostly confined to the target proton fragmentation region, i.e. to the c.m.s. backward hemisphere, but some data obtained in the beam fragmentation region are also used when an interesting comparison can be made.

As a first attempt to compare these results to current phenomenological ideas, we use the string fragmentation Lund model [2].

2. EXPERIMENTAL PROCEDURE

2.1 Event selection

The present study is based on the experiment NA 23 performed at CERN using the European Hybrid Spectrometer (EHS) and the Rapid Cycling Bubble Chamber (RCBC) exposed to a beam of protons at 360 GeV/c. A detailed description of the spectrometer and of the data acquisition has been published elsewhere [8,9].

The data used in this analysis are based on a sample of ~ 26 100 events. It includes a sample of ~ 10 700 events with at least one associated V^o (K^o_s, Λ^o or $\bar{\Lambda}^o$) or electron pair seen in the bubble chamber. The remaining ~ 15 400 events come from two different subsets: one of

them (~ 6200) corresponds to an unbiased sample of interactions, including the largest multiplicity events observed in the bubble chamber, the other one (~ 9200) is a sample of interactions with limited multiplicity ($\leq$ 12). Knowing the real multiplicity distribution for the non-biased sample, one can introduce appropriate weighting factors to compensate for the loss of unmeasured events with large multiplicities.

The interaction trigger used for on-line data acquisition has a good efficiency for events of interest for this analysis. To obtain a pure sample of fragmentation and central production events, we eliminate elastic events by removing those two-prong events which have a missing mass squared smaller than 2.5 GeV^2 and a momentum transfer squared smaller than 0.8 GeV^2. In addition, we eliminate all events where the fastest positive particle h^+ has Feynman-x greater than 0.85 provided that the rapidity gap between h^+ and the closest secondary particle is greater than 2.5. We considered only fully reconstructed events and tracks measured with a momentum precision better than 20%.

2.2 Mass assignments

To determine the masses of the charged particles used in the analysis, we make use of three sources of information: the bubble density which, if larger than 1.5 times minimum for tracks with momenta smaller than 1.4 GeV/c, indicates unambiguously that this track is due to a proton; the mass dependent geometry reconstruction program, which allows us to distinguish between the proton mass hypothesis and the π/K ones for most of the tracks with momenta smaller than 0.8 GeV/c; the particle identification given by a silica aerogel Cherenkov detector (SAD) [10] and a large pictorial drift chamber (ISIS) [11].

SAD is composed of 18 identical modules, each one having a sensitive surface of 23 x 55 cm^2 resulting in a total sensitive surface for the detector of 2.3 m^2. The threshold momentum is 0.56 GeV/c for π, 2.0 GeV/c for K and 3.8 GeV/c for protons. SAD is useful for particle identification in the momentum range 0.6 - 4.5 GeV/c. The reliability of the identification has been checked using kinematically fitted neutral particles (γ, K^o, Λ^o) and charged particles identified in ISIS.

For a charged track of given momentum passing through a SAD module, the theoretically expected numbers of photoelectrons for different masses are known. A χ^2-probability for the various mass assignments can be computed on the basis of this information using a previously determined calibration.

ISIS is equipped with 320 wires transverse to the beam, in a horizontal plane. It measures dE/dx from which the velocity of each track can be calculated. Combined with the momentum measurement, information on the mass of each particle passing through ISIS is obtained. This technique, which relies on the relativistic increase of ionisation in a gas, has been extensively reviewed [12] and its successful application in ISIS has been described elsewhere [11]. Briefly the sampling of the ionisation deposited by a particle traversing ISIS is made in up to 320 independent channels, with the regions of crossing tracks filtered out. This allows us to compute the ionisation distribution. This Landau distribution depends on a scale parameter [12] which is proportional to the energy lost by the particle traversing the Ar/CO_2 mixture. A maximum likelihood fit to determine an estimate of the value of this parameter for each track is performed giving the ionisation. The logarithm of the measured ionisation is normally distributed around the theoretical value, which can be computed if the momentum of the particle is known. This enables us to compute a χ^2-probability for each mass assignment. The ionisation resolution achieved is close to theoretical expectations. The particle identification has been checked by examining a large sample of tracks from reconstructed K^o and Λ^o decays and γ conversions observed in the bubble chamber during the course of this experiment. We found that electrons are uniquely resolved at the 1% level for momenta below 20 GeV/c, whereas for K/π separation the momentum range is 3-30 GeV/c.

SAD and ISIS provide particle identification in complementary momentum ranges. When both detectors give some information for a given track, a combined χ^2-probability is determined.

SAD and ISIS information was used for each track for which the χ^2 probability for at least one mass hypothesis was larger than 1%. Mass hypotheses whose probabilities were less than 0.5 of the largest probability were rejected.

In the case of a residual π/K ambiguity, we assign the π mass with a weight 0.9. In the case of a residual K/p ambiguity, we assign the proton mass to the track.

All tracks which remain totally ambiguous or for which we have no particle identification are assumed to be pions. The great majority of these tracks are from small |x| region ($|x| < 0.2$).

2.3 THE MODEL

The experimental results presented in this paper are compared to the predictions of the string fragmentation Lund model [2]. Therefore, the events generated by Lund Monte-Carlo are submitted to the same selection criteria as applied to the real events. The spectrometer acceptance and efficiency for individual tracks were taken into consideration. Using an ionization estimate and the track momentum, χ^2 probabilities were calculated for various mass assignments. The residual K and proton contamination in the "π" sample is therefore taken into account for the events generated by Lund Monte-Carlo and a meaningful comparison of the data with the model is possible since they are both affected in the same way by effects due to the limitations of particle identification.

3. RESULTS AND DISCUSSIONS

3.1 Invariant x distributions

The invariant Feynman x distributions

$$f(x) = \frac{2}{\pi\sqrt{s}} \int E \frac{d^2\sigma}{dx dp_T^2} dp_T^2$$

of π^+ and π^- are shown in fig. 1(a). Note that the π^+ distribution is affected by a residual contamination of protons and that the difference observed between the π^+ and the π^- may be partially due to this contamination all over the x_F range. In the proton fragmentation region both the π^+ and π^- x-distributions are well represented by a power law of the form $(1 - |x|)^n$. The curves correspond to Lund model predictions. The fitted values of the exponent n along with the values predicted by the Lund model are presented in table 1. (These values of n are obtained for the interval $0.2 < |x| < 0.7$).

As seen from table 1, Lund model predictions for n are slightly higher than the values derived from the data. Most of the models predict higher values of n for π^- as compared to π^+ in the proton fragmentation region.

Fig. 1(b) shows the x distributions of two pion systems $E_1 E_2 \, d\sigma/dx_{sum}$ where E_1, E_2 are the energies and $x_{sum} = x_1 + x_2$. For $|x| > 0.2$ the experimental data are well represented by the same functional form $(1 - |x_{sum}|)^n$ as the one used for single pion distributions. Again the Lund model tends to predict high values for n (table 1). The gluon exchange model [13] predicts values of the order of 7 and 9 for $\pi^+\pi^\pm$ and $\pi^-\pi^-$ respectively, in disagreement with the data.

The invariant x-distributions for three pion systems are shown in fig. 1(c) and the results of a power law fit are shown in table 1. The Lund model gives a reasonable description of the data whereas the gluon exchange model would predict steeper slopes.

In fig. 1(d) we present a comparison of the values obtained for the parameter n for various particle combinations from this experiment with other measurements obtained at different energies and with a variety of incident particles [7]. With the possible exception of n $(\pi^+\pi^+\pi^+)$ and n $(\pi^-\pi^-)$, one does not find any significant variation with the beam flavour or beam energy.

3.2 Particle ratios

The ratio of the inclusive invariant cross sections $R_1 = \sigma(\pi^+)/\sigma(\pi^-)$ for pions produced in proton fragmentation as a function of x is shown in fig. 2(a). This ratio increases gradually with x and seems to saturate at $R_1 \sim 3.5$ for x larger than 0.5. However, we remind the reader that there is a residual contamination of protons in the charged particles called π^+ here and in the following. This contamination may influence the shape of the π^+/π^- ratio as well as some of the other ratios discussed below.

In the fragmentation region, R_1 reflects the quantum numbers of the fragmenting hadron. Using the idea of single valence quark hadronization, this ratio should be equal to 2 in the proton fragmentation region. However the quark recombination picture [14] would predict that this ratio is approximately equal to $u_v(x)/d_v(x)$ at large x, i.e. values of the order of 5 as $x \to 1$ [15]. The two-chain DTU model of Capella [1] predicts that this ratio approaches 1.1 as x tends to 0.0, in good agreement with the data shown in fig. 2(a).

Fig. 2(b) shows the ratio of the inclusive invariant cross sections for $\pi^+\pi^-/\pi^+\pi^+$ and $\pi^+\pi^-/\pi^-\pi^-$ and a comparison of these results with the Lund model. The ratio $R(\pi^+\pi^-/\pi^+\pi^+)$ stays constant with a value ~ 1.5 over the entire x-region. As expected, the ratio $R(\pi^+\pi^-/\pi^-\pi^-)$ reaches much larger values as $x \to 1$. This increase of the ratio $R(\pi^+\pi^-/\pi^-\pi^-)$ can be explained in the following way: in the proton fragmentation region, only one of the π^- in a fast $\pi^-\pi^-$ system may contain a valence quark of the proton, whereas both particles of the $\pi^+\pi^-$ system may contain such quarks, leading to the suppression of the $\pi^-\pi^-$ system as compared to $\pi^+\pi^-$ for large values of x. The fragmentation of only one valence quark would yield a ratio $R(\pi^+\pi^-/\pi^-\pi^-) \to 2$ as $x \to 1$, in strong disagreement with the experimental observation.

The ratios $R(\pi^+\pi^-\pi^-/\pi^-\pi^-\pi^-)$ and $R(\pi^+\pi^-\pi^-/\pi^+\pi^+\pi^+)$ are presented in fig. 2(c). It is interesting to note that in the proton fragmentation region ($|x_{sum}| > 0.2$) the ratios $R(\pi^+\pi^-\pi^-/\pi^+\pi^+\pi^+)$ and $R(\pi^+\pi^-/\pi^+\pi^+)$ as well as $R(\pi^+\pi^-\pi^-/\pi^-\pi^-\pi^-)$ and $R(\pi^+\pi^-/\pi^-\pi^-)$ are approximately equal, as expected from a scheme with recombination of valence quarks. As seen from fig. 2(c), the ratio $R(\pi^+\pi^-\pi^-/\pi^+\pi^+\pi^+)$ ~ 1-2 has been found to be independent of x whereas $R(\pi^+\pi^-\pi^-/\pi^-\pi^-\pi^-)$ shows a strong x dependence. This can be explained again by the assumption that, in the fast $(\pi^+\pi^-\pi^-)$ and $(\pi^+\pi^+\pi^+)$ systems, two of the pions can contain a valence quark, whereas only one pion can be associated to a valence quark in the $(\pi^-\pi^-\pi^-)$ system.

The ratios $R(\pi^+\pi^+\pi^-/\pi^+\pi^-\pi^-)$, $R(\pi^+\pi^+\pi^-/\pi^+\pi^+\pi^+)$ and $R(\pi^+\pi^+\pi^-/\pi^-\pi^-\pi^-)$ are presented in fig. 2(d). One can see that the ratio $R(\pi^+\pi^+\pi^-/\pi^-\pi^-\pi^-)$ increases very rapidly with increasing |x| whereas the ratios $R(\pi^+\pi^+\pi^-/\pi^+\pi^-\pi^-)$ and $R(\pi^+\pi^+\pi^-/\pi^+\pi^+\pi^+)$ show no strong x dependence. One could have expected

some |x| dependence for these ratios since in the fast $(\pi^+\pi^+\pi^-)$ system all three pions can contain simultaneously one valence quark whereas, only two pions can contain a valence quark in the $(\pi^+\pi^-\pi^-)$ and $(\pi^+\pi^+\pi^+)$ systems. The difference in magnitude of the ratio $R(\pi^+\pi^+\pi^-/\pi^+\pi^+\pi^+)$ and $R(\pi^+\pi^+\pi^-/\pi^+\pi^-\pi^-)$ may be explained by arguing that fast $(\pi^+\pi^-\pi^-)$ systems are easier to form than fast $(\pi^+\pi^+\pi^+)$ since fast π^+ may come from either of the two valence quarks u of the proton.

The Lund model gives a good interpretation of all these distributions.

3.3 Particle production in association with a leading $\pi^\pm$

In the proton fragmentation region, particle production can be studied in association with various leading trigger particles [16], i.e. one selects interactions in which a particle of given nature is observed in the backward hemisphere with the largest |x| value and also |x| > 0.2. One expects that with a π^+ trigger, one u valence quark of the proton is removed and the remaining u and d valence quarks should produce equal amounts of π^+ and π^- at a fixed

$$x' = \left(\frac{x}{1 - |x_{tr}|}\right).$$

x_{tr} is the Feynman x value of the trigger particle. This is confirmed by the data in fig. 3, where the ratio $R(\pi^+/\pi^-)$ appears to be constant and close to 1 in the whole x' region for a π^+ trigger.

Similarly, with a π^- trigger, the remaining valence quarks in the proton fragmentation should produce more π^+ than π^-. Thus the ratio $R(\pi^+/\pi^-)$ in such a case shows a strong increase with x' (fig. 3). This ratio has been studied for various x_{tr} region of the trigger particle (fig. 4) and its qualitative behaviour agrees with the above expectations.

A comparison with similar information obtained with 70 GeV/c K^+p interactions (Barth [7]) shows neither energy nor beam flavour dependence.

The Lund model gives a good interpretation of the data.

The extended quark recombination model predicts also $R(\pi^+/\pi^-) \simeq 1$ for the π^+ trigger, and predicts for the π^- trigger that $R(\pi^+/\pi^-)$ should evolve from ~ 1 at small values of x' to u_v/d_s when x' tends towards 1. (u_v is for "valence quark u", d_s is for "sea quark d").

3.4 The p_T dependence of particle ratios

An interesting aspect of the study of particle ratios is to look for their p_T dependence, since it may provide information about the geometrical distribution of valence quarks in the proton. In general low p_T scattering takes place with the peripheral partons. Therefore mesons originating at the centre would have larger p_T values than those produced from more peripheral partons [17, 3]. If we assume that the proton contains a tightly bound ud diquark geometrically confined to small distances from the center, and a u quark orbiting around it [15,18], one expects that the ratio $R(\pi^+/\pi^-)$ should decrease with p_T.

Fig. 5(a) shows the p_T dependence of $R(\pi^+/\pi^-)$ for different values of x, in the forward hemisphere, where the amount of wrongly identified particles has been reduced to a low level by requiring that the π^+ and π^- are the only mass assignments giving a probability larger than 1% in ISIS. The events generated by Lund Monte-Carlo, applying these stringent criteria for particle identification, reproduce quite well the experimental data and do not exhibit a significant variation with p_T. If we consider the particles emitted in the backward hemisphere, and apply the relatively less stringent particle identification described in sect. 2, we obtain the distribution shown in fig. 5(b). The enhancement at medium x values is due to the residual proton contamination in the π^+ sample. This observation seems to be common to several experiments [19,20,21]. The Lund fragmentation model, which includes our selection rules for particle identification, reproduces quite well this behaviour of the experimental data.

3.5 Particle ratios of strange and non-strange mesons

The particle ratios $R(\pi^+/K^o_s)$ and $R(\pi^-/K^o_s)$ have been measured as a function of x (fig. 6). The production of a fast K^o_s should be associated to $\bar{s}_s\, d_v$ (s_s for antistrange quark from the sea, d_v being the valence

quark d) and slow K^o_s to $\bar{s}_s\, d_s$ and $s_s\, \bar{d}_s$. At large |x|, the ratio $R(\pi^-/K^o_s)$ is related to the ratio $\bar{u}_s/\bar{s}_s$. It is found to be close to 3.5, in agreement with the standard strangeness suppression factor of ~ 0.3. The Lund fragmentation model, which assumes a suppression factor of 0.3, gives a good interpretation of the data in the proton fragmentation region. This agreement seems to be lost in the more central region.

At large |x|, the ratio $R(\pi^+/K^o_s)$ should be given by $(u_v/d_v)\,.\,(d_s/s_s)$. The first term is given by $R(\pi^+/\pi^-)$ at large |x| obtained with a K^o_s trigger; it is found to be close to 7 in our experiment (see fig. 7(b)). The second term is given by the strangeness suppression factor, i.e. ~ 3.5. One therefore expects that $R(\pi^+/K^o_s)$ tends to ~ 25 at large |x|, in agreement with fig. 6(b).

The behaviour of these ratios also suggests that K^o production dominates over $\bar{K}^o$, at large |x|.

3.6 Particle production ratios in association with a leading Λ^o or K^o_s

An analysis of the particle ratio $R(\pi^+/\pi^-)$ in association with a strange particle trigger (Λ^o or K^o_s) in the proton fragmentation region can provide some information on the quark structure of the proton. With a Λ trigger, the u and d valence quarks are taken away simultaneously: one therefore expects that the ratio $R(\pi^+/\pi^-)$ will increase with |x'|. It should also be a factor two smaller than the same ratio with a π^- trigger. The data confirm this picture fig. 7(a) and the Lund fragmentation model provides a good interpretation of the experimental distribution.

In the case of a K^o_s trigger (as with a fast π^- trigger) the valence quark taken away is a d quark, and the ratio $R(\pi^+/\pi^-)$ should reflect, at large x' values, the properties of the left over valence quarks in the proton i.e. the two u quarks. However, it is known that a large fraction of the K^o_s come from the decay of $K^*(892)$ [22], which may spoil this picture. Fig. 7(b) shows the strong dependence of $R(\pi^+/\pi^-)$ with x' for the K^o_s trigger data.

Fig. 8 shows the x' dependence of $R(\pi^+/\pi^-)$ associated with a Λ^o, K^o_s or π^- trigger. The ratios $R(\pi^+\pi^-/\pi^-\pi^-)$, $R(\pi^+\pi^-\pi^-/\pi^-\pi^-\pi^-)$ and $R(K^+/K^-)$ are also displayed on the same figure. The ratio $R(K^+/K^-)$ is computed for the c.m.s. forward hemisphere where we have acces to some K^+ and K^- identification. All these ratios where similar valence quarks play an important role are in good agreement with each other, particularly in the proton fragmentation region ($|x| > 0.2$).

4. SUMMARY AND CONCLUSION

In this paper we have studied inclusive particle production ratios in pions and pion systems at 360 GeV/c in pp interactions. The results have been quantitatively compared with predictions of the Lund fragmentation model. The main results of the study may be summarized as follows:

- The invariant Feynman x-distributions of the single, double- and triple-pion systems are described by a $(1 - |x|)^n$ power law behaviour in the $|x| \geq 0.2$ region. These distributions, as well as the particle ratios for pions or pion systems and the ratios $R(\pi^+/\pi^-)$ obtained in association with a π^+ or π^- trigger are well reproduced by a simple string fragmentation (Lund) model.

- No significant dependence of $R(\pi^+/\pi^-)$ on p_T is observed.

- The x-dependence of $R(\pi^+/K^o)$ and $R(\pi^-/K^o)$ in proton fragmentation are in agreement with the Lund model. The analysis seems also favour the dominance of K^o over $\bar{K}^o$ in the large x-region.

- Results on the x-dependence of $R(\pi^+/\pi^-)$ in association with a trigger Λ^o or K^o_s are in qualitative agreement with the simple quark recombination picture.

- In the proton fragmentation region the x-dependence of particle ratios such as $R(\pi^+/\pi^-)$ with π^-, K^o_s or Λ^o trigger and also $R(\pi^+\pi^-/\pi^-\pi^-)$, $R(\pi^+\pi^-\pi^-/\pi^-\pi^-\pi^-)$ and $R(K^+/K^-)$ have the same behaviour. This is in agreement with the assumption that all these ratios reflect the behaviour of the ratio q_v/q_s (valence quark to sea quark) in the proton. Therefore it seems likely that each of the systems $(\pi^+\pi^-)$ and $(\pi^+\pi^-\pi^-)$ contain frequently two valence quarks.

In conclusion, we observe that the hypothesis that soft hadron production at $|x| > 0.2$ probes the constituent nature of the colliding hadrons has been successfully tested on data obtained with proton proton interactions at 360 GeV/c. The results are in agreement with the current valence - sea quark picture of the proton. Further refinements of this picture have been proposed, with the introduction of a quark-diquark composition of the proton [18]. The results presented here are not sensitive to these refinements and do not indicate that, if a diquark is present, its geometrical distribution in the proton is different from the valence quark.

Acknowledgements

We are indebted to the CERN staff, whose sterling performance was essential in collecting the data for this experiment. We also would like to take the opportunity to acknowedge the heroic effort by our scan and measurement personel in the participating labs and Miss M. King for invaluable assistance in typing this paper.

REFERENCES

[1] A. Capella, Proc. Europhysics study conf. on partons in soft hadronic processes, Erice, ed. R.T. Van de Walle, (Singapore: World Scientific) p. 199 (1981).

[2] T. Sjöstrand, LUND preprint LUTP 82-3, (1982);
B. Andersson et al., Phys. Rep. 97 (1983) 33;
T. Sjöstrand, Computer Phys. Comm. 27 (1982) 243;
T. Sjöstrand, Computer Phys. Comm. 28 (1983) 229.

[3] J. Gunion, Proc. Europhysics study conf. on partons in soft hadronic processes, Erice, ed. R.T. Van de Walle, (Singapore: World Scientific) p. 293 (1981).

[4] R. Hwa, Proc. Europhysics study conf. on partons in soft hadronic processes, Erice, ed. R.T. Van de Walle, (Singapore: World Scientific) p. 137 (1981).

[5] V.V. Anisovich et al., Zeitsch. für Phys. C27 (1985) 87.

[6] K. Fialkowski and W. Kittel, Rep. Prog. Phys. 46 (1983) 1283.

[7] K.W. Barnham, Proceedings of the EPS conf. on High Energy Physics, Geneva 1979;
W. Lockman et al., Phys. Rev. Lett. 41 (1978) 680;
E.A. de Wolf et al., Zeitsch. für Physik C8 (1981) 189;
U. Gensch et al., Zeitsch. für Physik C17 (1983) 21;
M. Barth et al., Zeitsch. für Physik C7 (1981) 187;
R. Göttgens et al., Zeitsch. für Physik C22 (1984) 205.

[8] J.L. Bailly et al., Zeitsch. für Phys. C, Particles and Fields 22 (1984) 119.

[9] M. Asai et al., Zeitsch. für Phys. C, Particles and Fields 27 (1985) 11.

[10] P.J. Carlsson et al., Nucl. Instr. Methods 204 (1982) 65.

[11] W.W. Allison et al., Nucl. Instr. Methods 224 (1984) 396.

[12] W.W. Allison et al., Annual Rev. Nucl. Part. Science 39 (1980) 253.

[13] S.J. Brodsky and J.F. Gunion, Phys. Rev. D17 (1978) 848;
J.F. Gunion, Phys. Lett. 88B (1979) 150.

[14] E. Takasugi and X. Tata, Phys. Rev. D21 (1980) 1838;
E. Takasugi and X. Tata, Phys. Rev. D23 (1981) 2573;
E. Takasugi and X. Tata, Phys. Rev. D26 (1982) 120.

[15] G.R. Farrar and J.D. Jackson, Phys. Rev. Lett. 35 (1975) 1416.

REFERENCES (Cont'd)

[16] E. Lehman et al., Phys. Rev. D18 (1978) 3353.

[17] R. Feynman, R.D. Field and G. Fox, Nucl. Phys. B128 (1977) 1.

[18] J.L. Bailly et al., Zeitsch. für Phys. C31 (1986) 367.

[19] M. Abramowich et al., Zeitsch. für Phys. C7 (1981) 199.

[20] I.V. Ajinenko et al., Zeitsch. für Phys. C4 (1980) 181.

[21] D. Brick et al., Zeitsch. für Phys. C13 (1982) 11.

[22] T. Aziz et al., Zeitsch. für Phys. C30 (1986) 381.

TABLE 1

Particles	Exponent n	
	Experimental	Lund model
π^+	3.3 ± 0.3	4.2 ± 0.2
π^-	3.9 ± 0.3	4.5 ± 0.3
$\pi^+\pi^+$	3.2 ± 0.1	3.8 ± 0.1
$\pi^+\pi^-$	2.9 ± 0.1	3.2 ± 0.1
$\pi^-\pi^-$	3.6 ± 0.1	4.2 ± 0.3
$\pi^+\pi^+\pi^+$	2.5 ± 0.1	2.5 ± 0.1
$\pi^+\pi^+\pi^-$	2.5 ± 0.1	2.5 ± 0.1
$\pi^+\pi^-\pi^-$	2.7 ± 0.1	2.4 ± 0.1
$\pi^-\pi^-\pi^-$	3.3 ± 0.2	2.3 ± 0.1

FIGURE CAPTIONS

Fig. 1 (a) Feynman-x distribution of the π^+ and π^- invariant cross sections.

(b) Feynman $x_{sum} = x_1 + x_2$ distribution of the invariant cross sections of two pion systems (arbitrary unit).

(c) Feynman $x_{sum} = x_1 + x_2 + x_3$ distribution of the invariant cross sections of three pion systems (arbitrary unit).

The smooth curves are the predictions of the Lund model.

(d) Values of the parameter n obtained at different energies and with various beam flavours.

Fig. 2 Ratio of invariant cross section of one-pion, two-pion and three pion systems vs Feynman-x. The smooth curves are the predictions of the Lund model.

Fig. 3 π^+ to π^- invariant cross section ratio vs x' in association with a leading π^+ or π^- The smooth curves are the predictions of the Lund model.

Fig. 4 π^+ to π^- invariant cross section ratio vs x' in association with a π^- trigger for different regions of x_{tr} (x of the trigger particle). The smooth curves are the predictions of the Lund model.

Fig. 5 (a) π^+ to π^- invariant cross section ratio for non ambiguously identified π^+ and π^- vs p_T (forward hemisphere).

(b) π^+ to π^- invariant cross section ratio vs p_T for different regions of x (backward hemisphere).

The smooth curves are the predictions of the Lund model.

FIGURE CAPTIONS (Cont'd)

Fig. 6 (a) π^- to K_s^o invariant cross section ratio vs Feynman-x.

(b) π^+ to K_s^o invariant cross section ratio vs Feynman-x.

The smooth curves are the predictions of the Lund model.

Fig. 7 π^+ to π^- invariant cross section ratio vs x' in association (a) with a Λ-trigger, (b) with a K_s^o trigger. The smooth curves are the predictions of the Lund model.

Fig. 8 Comparison of the production ratios of various particles and systems of particles vs Feynman $|x|$.

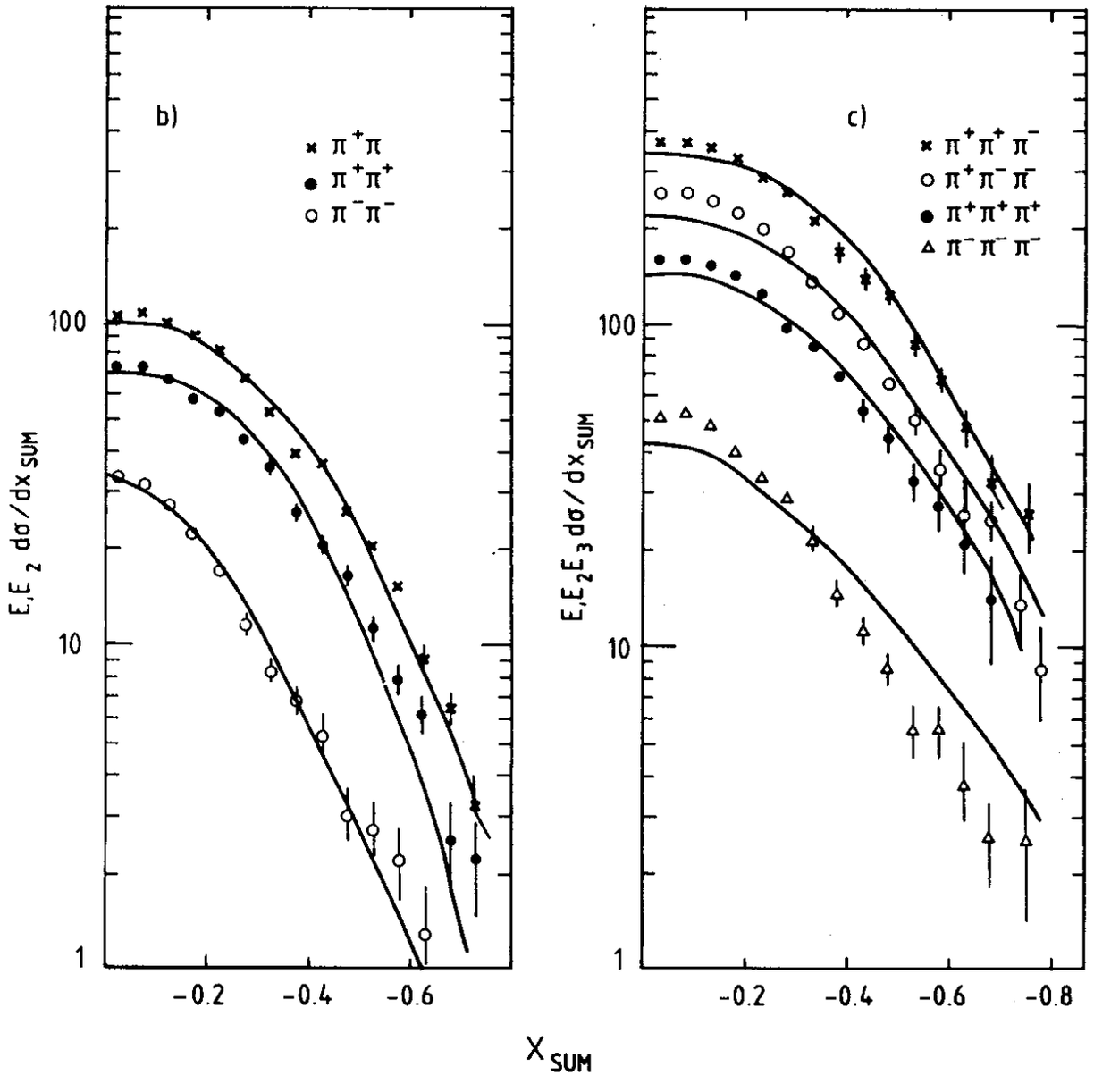
b)
$\pi^+\pi$
$\pi^+\pi^+$
$\pi^-\pi^-$
c)
$\pi^+\pi^+\pi^-$
$\pi^+\pi^-\pi^-$
$\pi^+\pi^+\pi^+$
$\pi^-\pi^-\pi^-$
100
10
1
$E_1 E_2 \, d\sigma/dx_{SUM}$
$E_1 E_2 E_3 \, d\sigma/dx_{SUM}$
-0.2
-0.4
-0.6
-0.8
X_{SUM}

FIG. 1

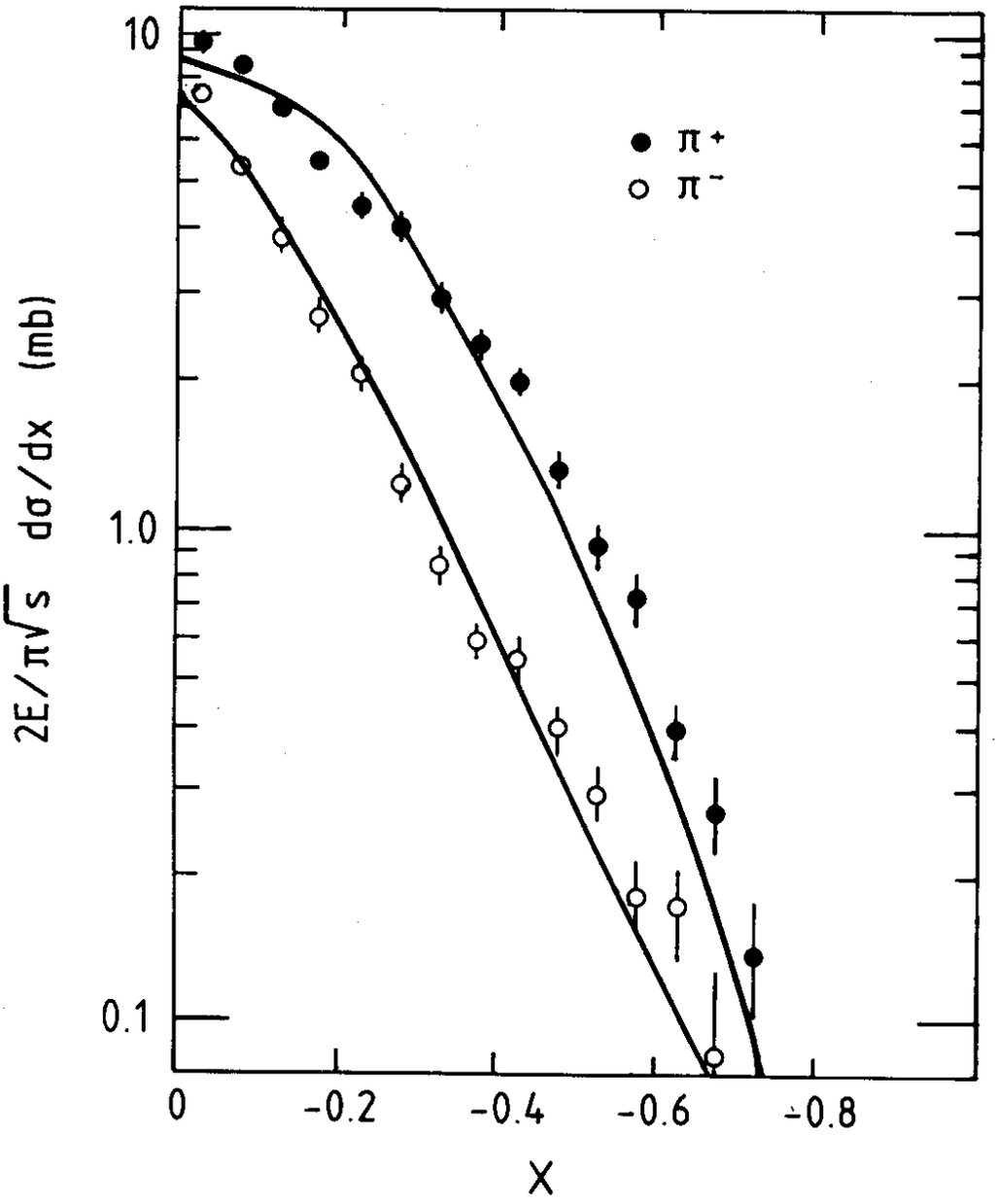

FIG. 1a

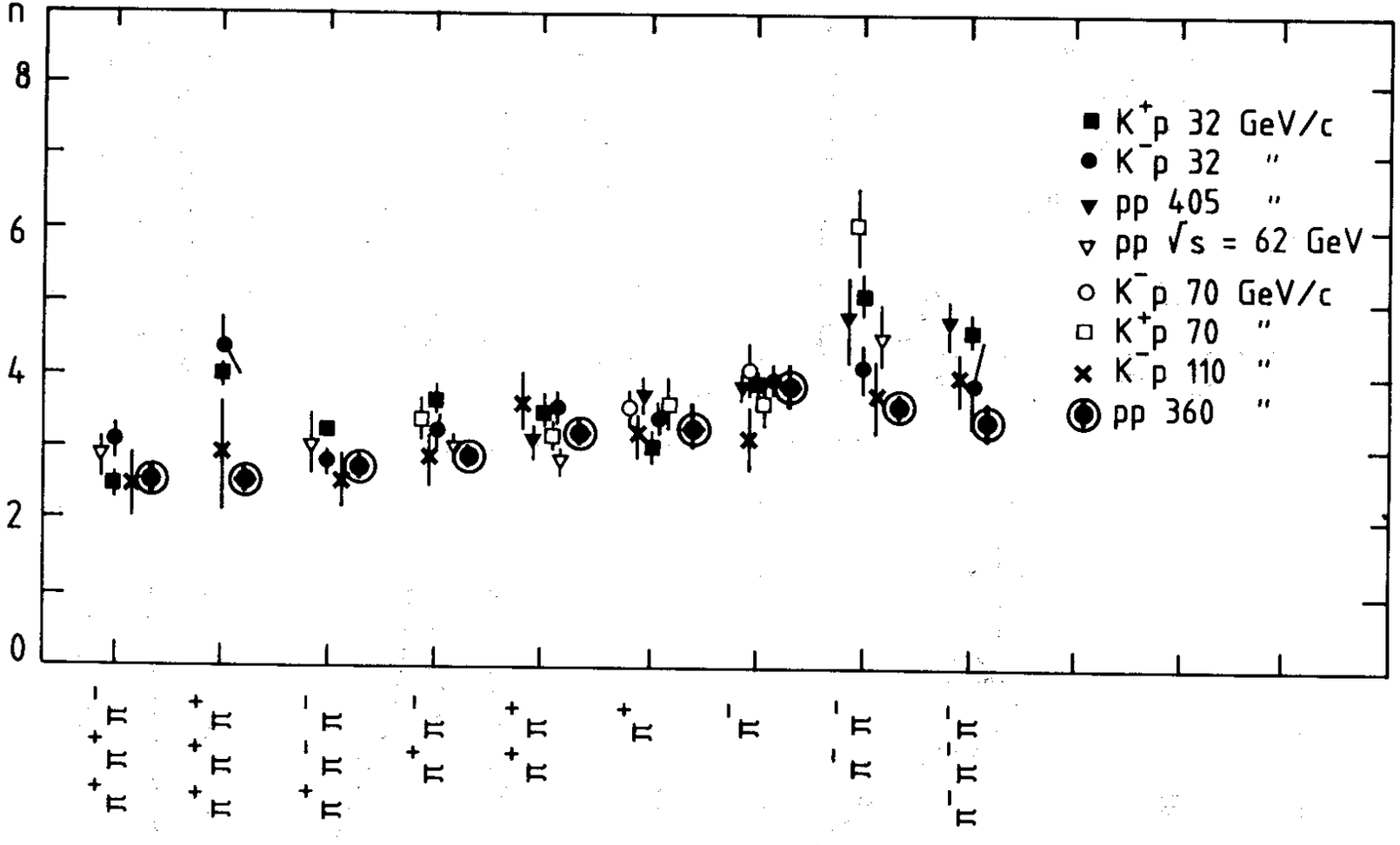
n
8
6
4
2
0
K+p 32 GeV/c
K−p 32 "
pp 405 "
pp √s = 62 GeV
K−p 70 GeV/c
K+p 70 "
K−p 110 "
pp 360 "
π+ π+ π− π−
π+ π+ π+ π−
π+ π− π+ π−
π+ π− π−
π+ π+ π−
π+ π−
π+ π−
π− π−
π− π+ π−

FIG. 1d

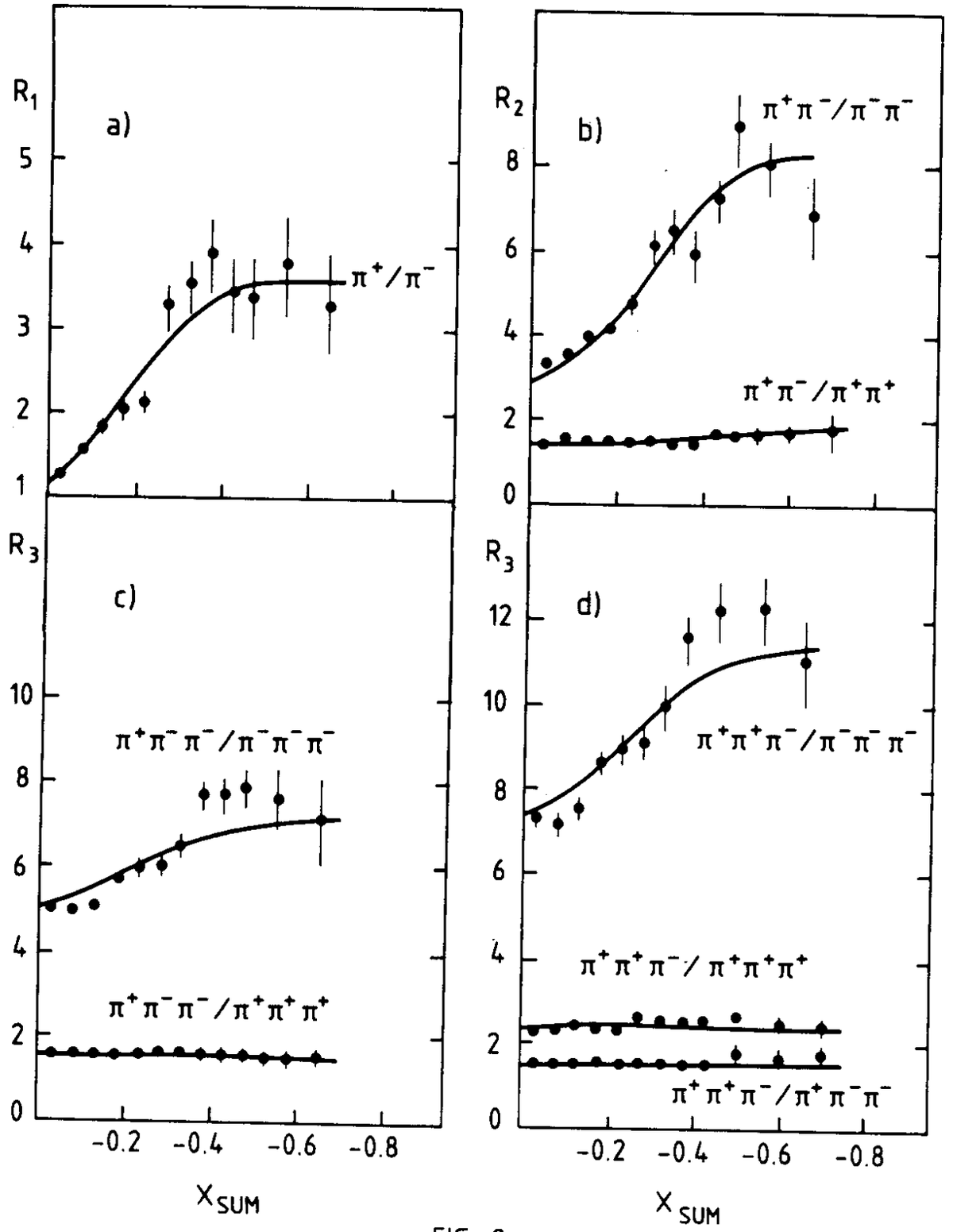
a)
R_1
π^+/π^-
b)
R_2
$\pi^+\pi^-/\pi^-\pi^-$
$\pi^+\pi^-/\pi^+\pi^+$
c)
R_3
$\pi^+\pi^-\pi^-/\pi^-\pi^-\pi^-$
$\pi^+\pi^-\pi^-/\pi^+\pi^+\pi^+$
d)
R_3
$\pi^+\pi^+\pi^-/\pi^-\pi^-\pi^-$
$\pi^+\pi^+\pi^-/\pi^+\pi^+\pi^+$
$\pi^+\pi^+\pi^-/\pi^+\pi^-\pi^-$
X_{SUM}
X_{SUM}

FIG. 2

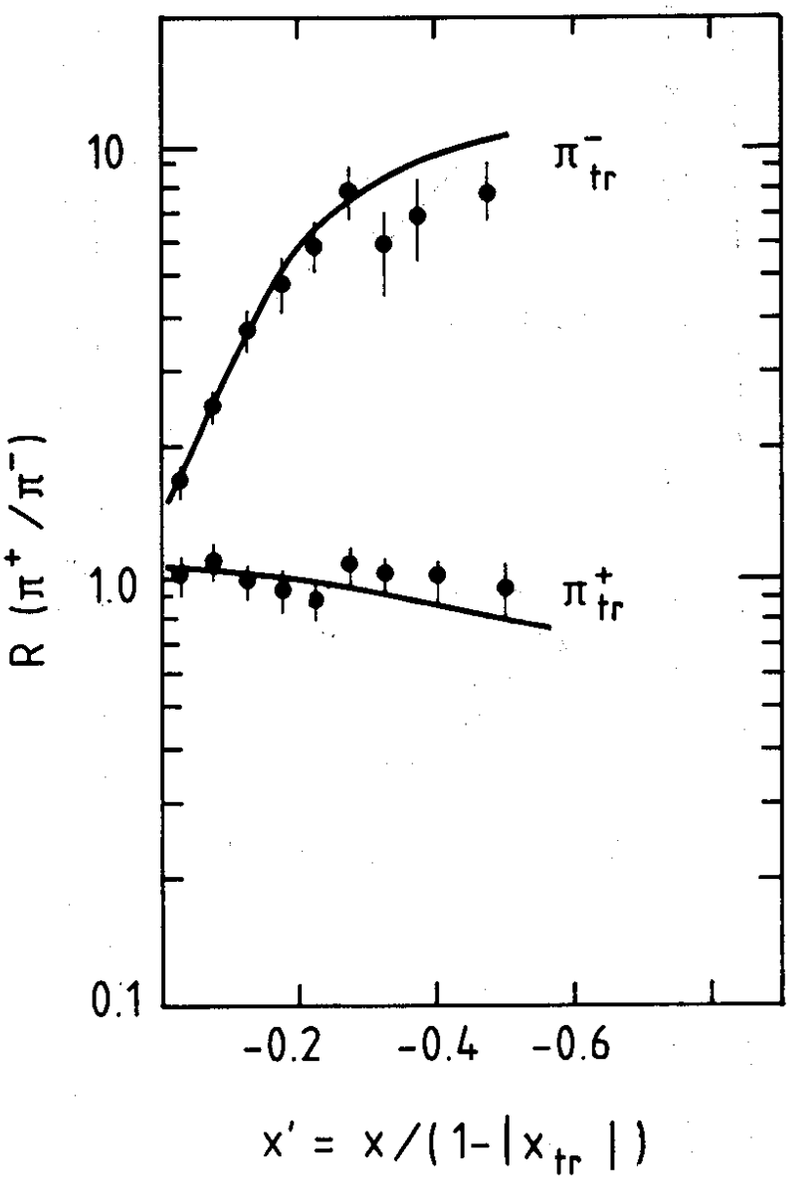

FIG. 3

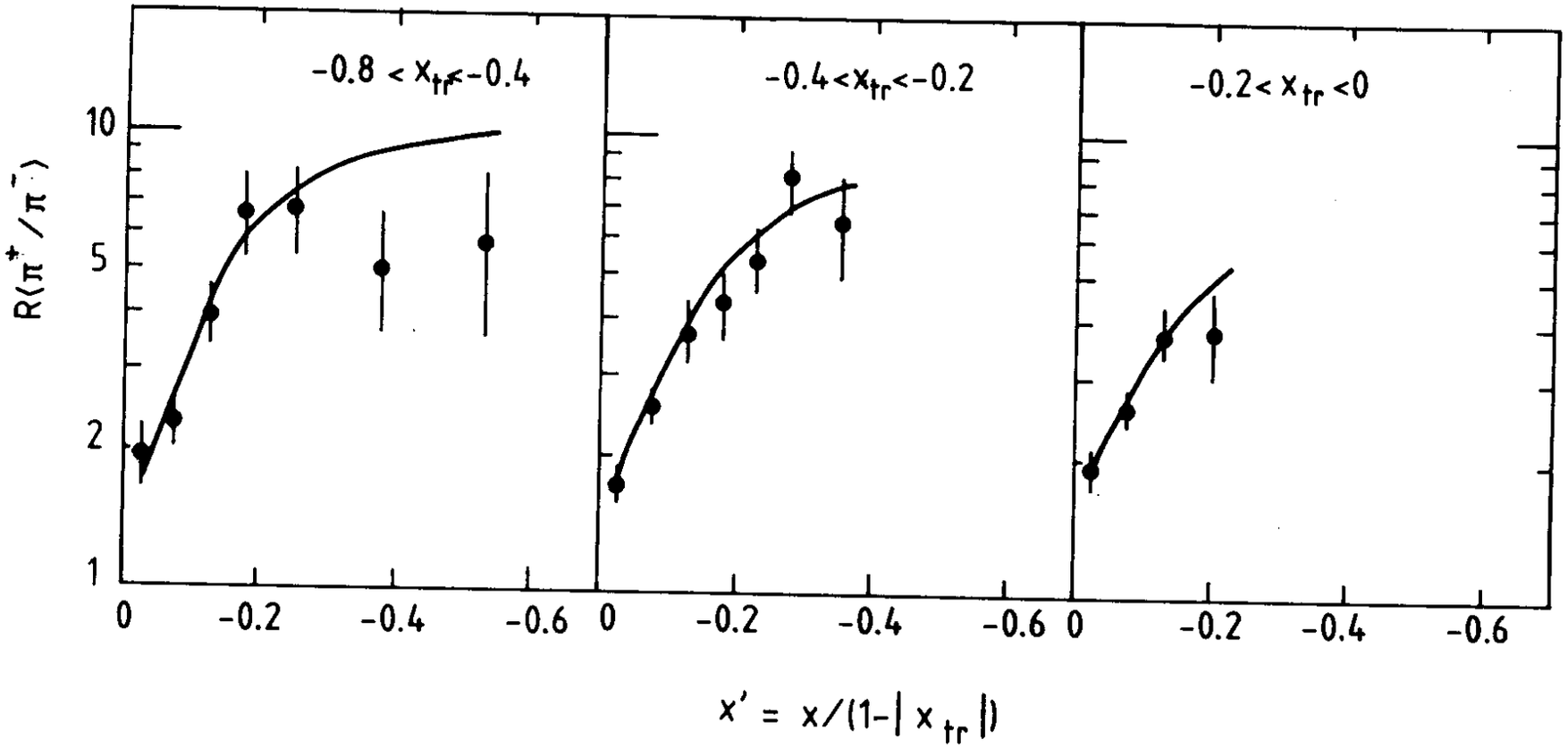

FIG. 4

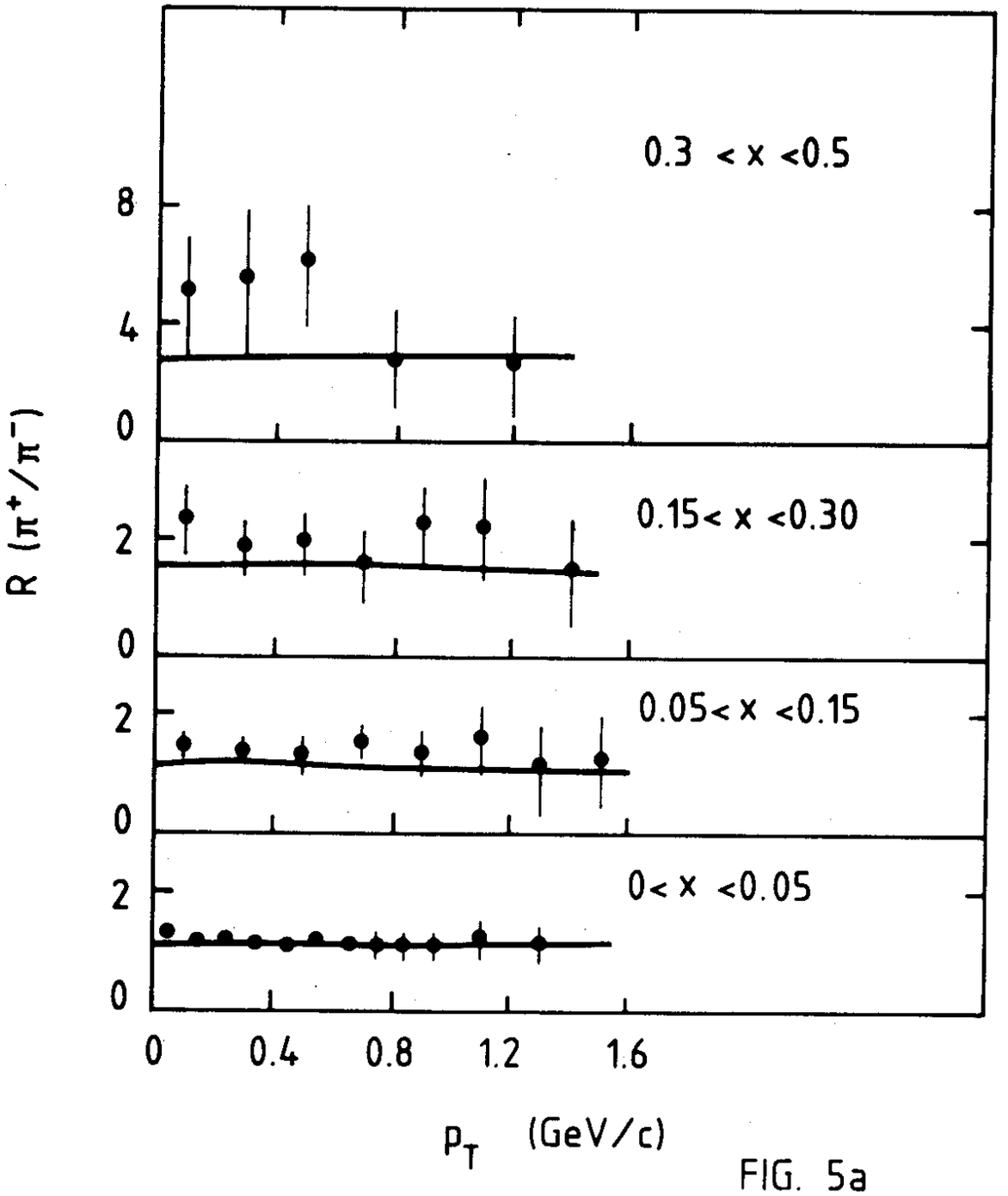
0.3 < x <0.5
0.15< x <0.30
0.05< x <0.15
0< x <0.05
R (π⁺/π⁻)
8
4
0
2
0
2
0
2
0
0
0.4
0.8
1.2
1.6
p_T (GeV/c)

FIG. 5a

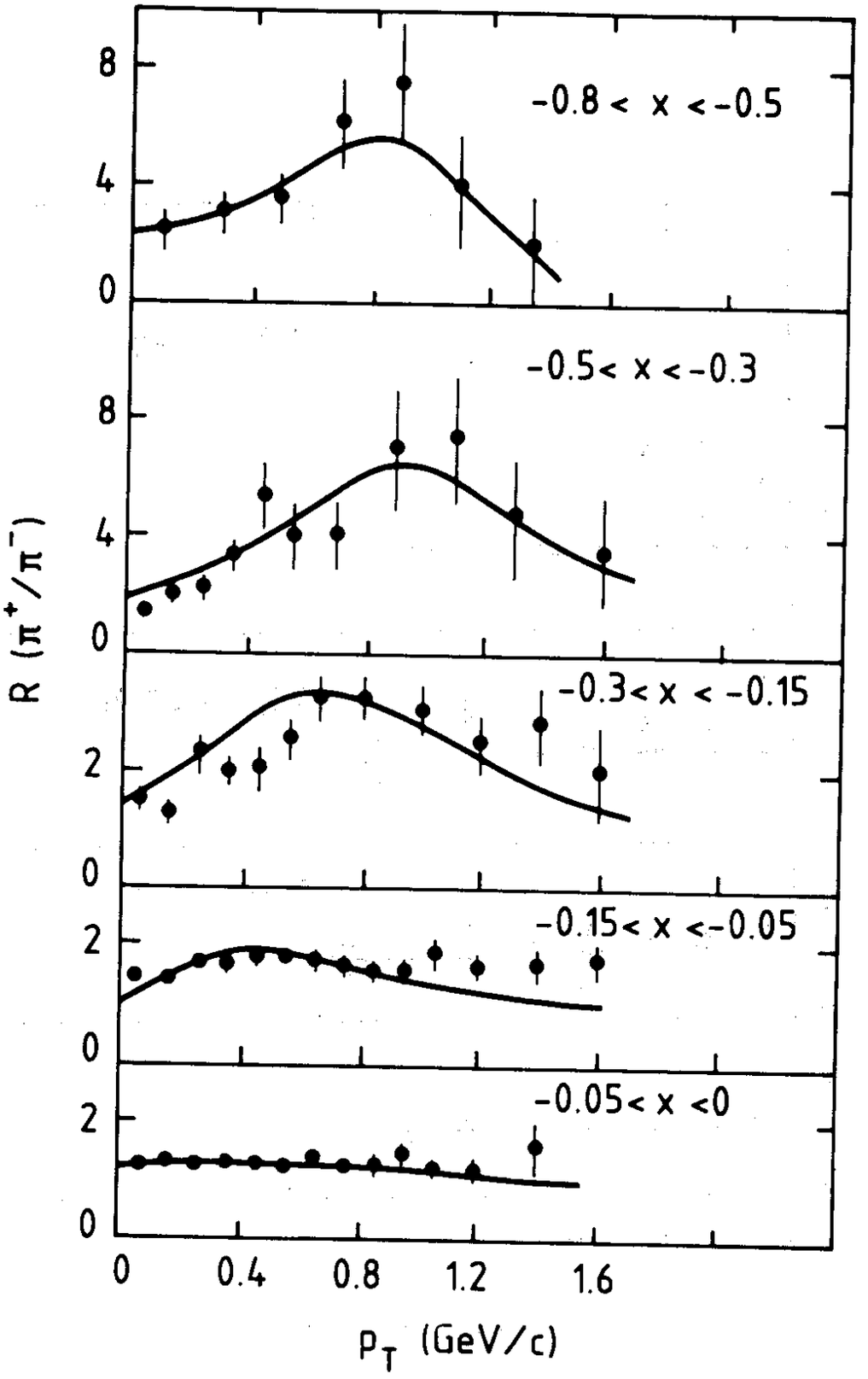

FIG. 5b

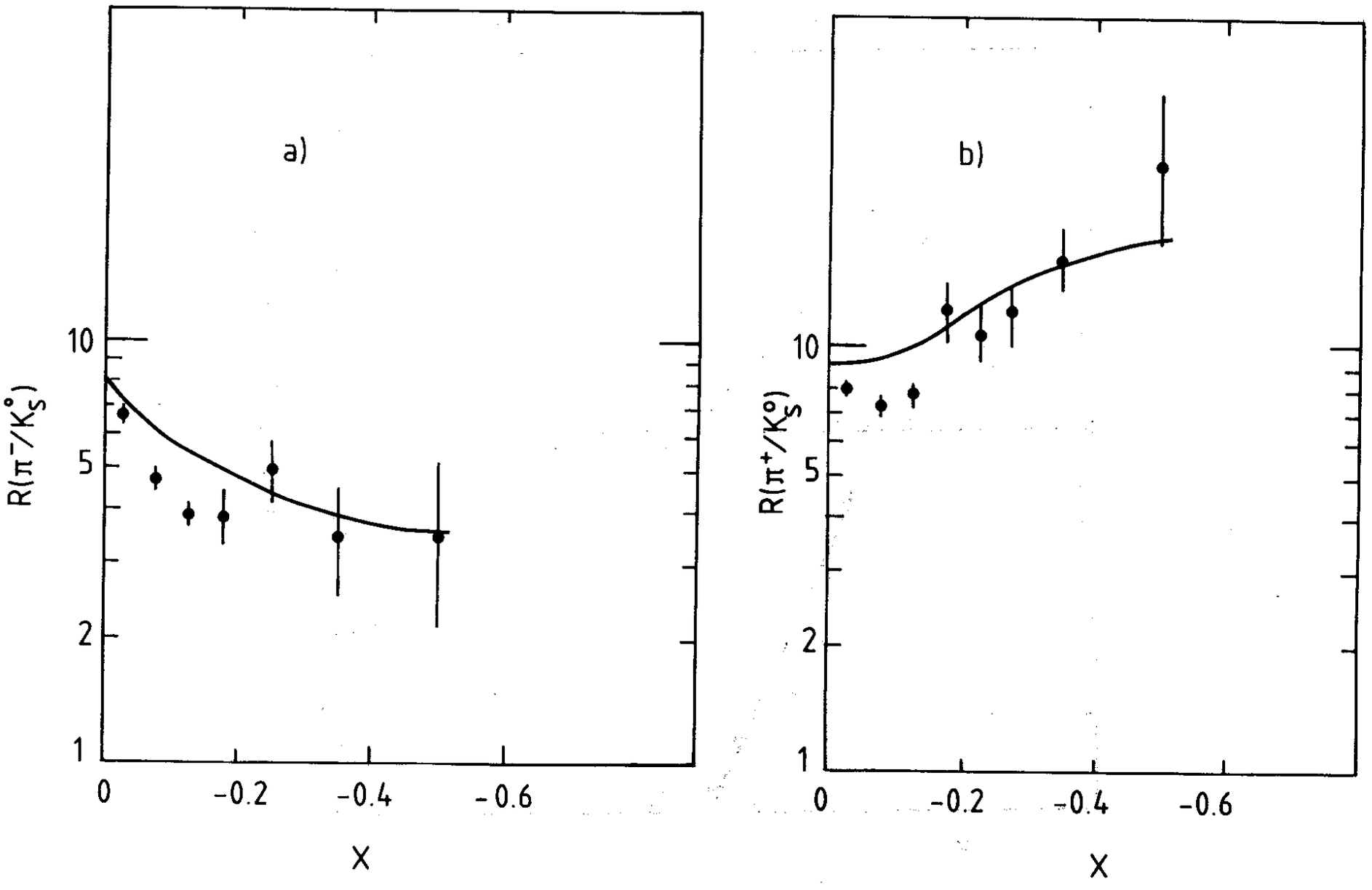

FIG. 6

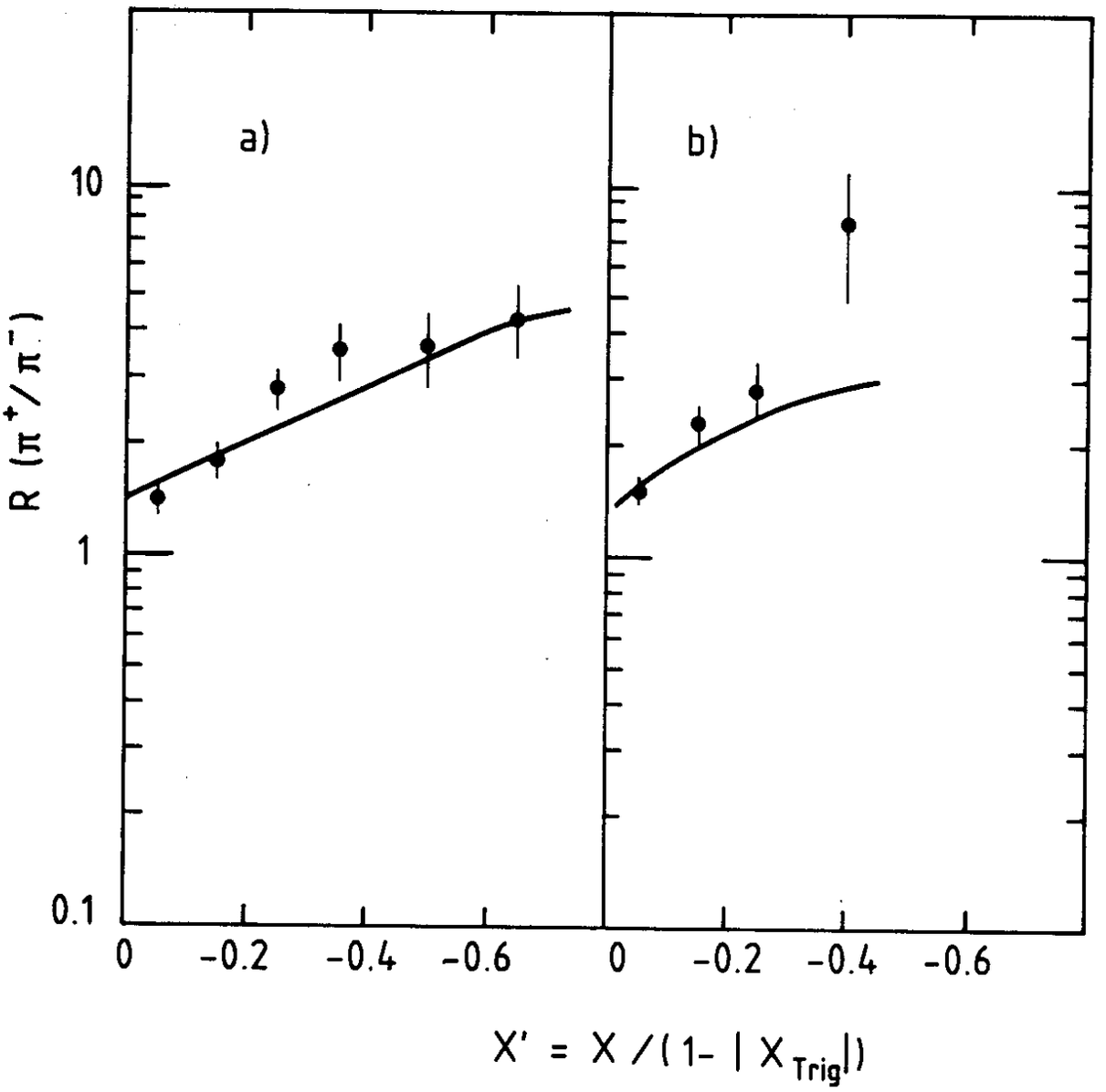

FIG. 7

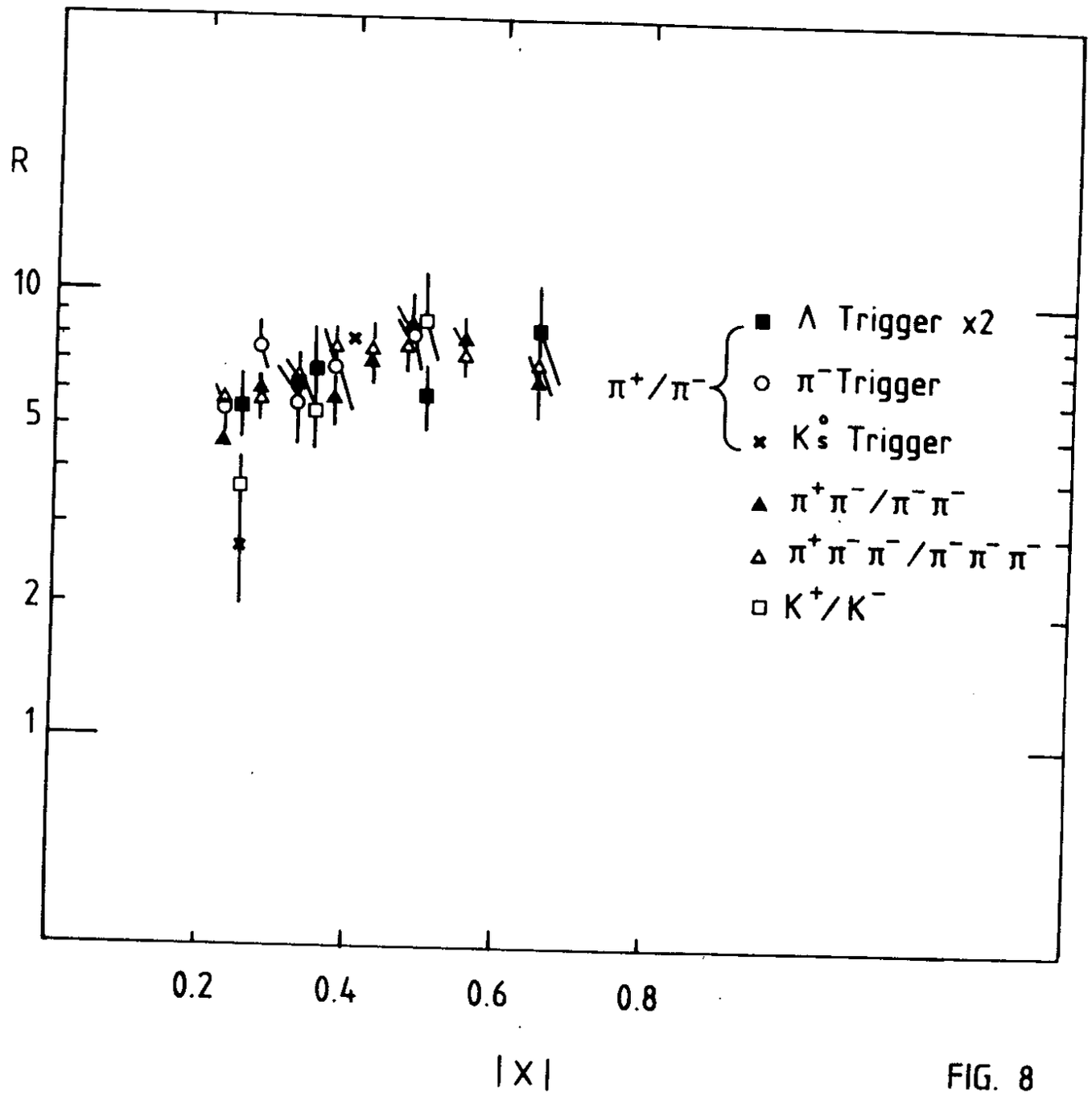
R
10
5
2
1
0.2
0.4
0.6
0.8
|X|
π+/π−
Λ Trigger x2
π− Trigger
K°s Trigger
π+π−/π−π−
π+π−π−/π−π−π−
K+/K−

FIG. 8